Instability of the roll-streak structure induced by background turbulence in pretransitional Couette flow

Brian F. Farrell

School of Engineering and Applied Science, Harvard University, Cambridge, Massachusetts 02138, USA

Petros J. Ioannou[*] and Marios-Andreas Nikolaidis

Department of Physics, National and Kapodistrian University of Athens, Athens 157 72, Greece

Although the roll-streak structure is ubiquitous in both observations and simulations of pretransitional wall-bounded shear flow, this structure is linearly stable if the idealization of laminar flow is made. Lacking an instability, the large transient growth of the roll-streak structure has been invoked to explain its appearance as resulting from chance occurrence in the background turbulence of perturbations configured to optimally excite it. However, there is an alternative interpretation for the role of free-stream turbulence in the genesis of the roll-streak structure, which is that the background turbulence interacts with the roll-streak structure to destabilize it. Statistical state dynamics (SSD) provides analysis methods for studying instabilities of this type that arise from interaction between the coherent and incoherent components of turbulence. SSD in the form of a closure at second order is used in this work to analyze the cooperative eigenmodes arising from interaction between the coherent streamwise invariant component and the incoherent background component of turbulence. In pretransitional Couette flow a manifold of stable modes with roll-streak form is found to exist in the presence of low-intensity background turbulence. The least stable mode of this manifold is destabilized at a critical value of a parameter controlling the background turbulence intensity and a finite-amplitude roll-streak structure arises from this instability through a bifurcation in this parameter. Although this bifurcation has analytical expression only in the infinite ensemble formulation of second order SSD, referred in this work as the S3T system, it is closely reflected in numerical simulations of both the dynamically similar quasilinear system, referred to as the restricted nonlinear (RNL) system, as well as in the full Navier-Stokes equations. This correspondence is verified using ensemble implementations of the RNL system and the Navier-Stokes equations. The S3T system also predicts a second bifurcation at a higher value of the turbulent excitation parameter that results in destabilization of the finite-amplitude roll-streak equilibria. This second bifurcation is shown to lead first to time dependence of the roll-streak structure in the S3T system and then to chaotic fluctuation corresponding to minimal channel turbulence. This transition scenario is also verified in simulations of the RNL system and of the Navier-Stokes equations. This bifurcation from a finite-amplitude roll-streak equilibrium provides a direct route to the turbulent state through the S3T roll-streak instability.

I. INTRODUCTION

Streamwise roll vortices and associated streamwise streaks were identified in experiments on transition in boundary layers [1] and observed in the near-wall region of turbulent flows [2–4]. These observations were subsequently corroborated by direct numerical simulations (DNSs) (see [5]) and the roll-streak structure is now understood to be central to the dynamics of turbulence in wall-bounded shear flows.

---

[*]pjioannou@phys.uoa.gr

There are two distinct dynamical problems central to understanding wall turbulence: transition from the laminar to the turbulent state and maintenance of the turbulent state. The roll-streak structure, despite being hydrodynamically stable, is commonly agreed to be involved in instigating transition from the laminar to the turbulent state in these flows. After transition this structure persists but becomes highly variable in both space and time. This time-dependent streamwise roll and streak structure is believed to be involved in the process maintaining turbulence in shear flow that is referred to as the self-sustaining process [6–9]. Moreover, this self-sustaining mechanism appears to be quite general in that it operates not only in the near-wall region but also, and independently, in the logarithmic layer [10,11].

Our primary interest in this work is in the robust observation of the roll-streak structure in wall-bounded shear flow prior to transition and in understanding the role of this structure in the transition process. The prominence of the roll-streak structure in these flows presents a problem because this structure is not an unstable eigenmode of the shear flow existing prior to transition. The robust observation of the roll-streak structure was first rationalized by appeal to the lift-up mechanism that describes the kinematic conversion of wall normal velocity into streamwise streak velocity in sheared flows [12,13]. This insight was later advanced by recognition that the lift-up mechanism could be subsumed into the analytical structure of generalized stability theory (GST) by which modal stability theory and non-normal transient growth analysis are united [14–16]. While modal stability analysis provides no reason to expect the appearance of roll-streak structures, GST analysis predicts optimally growing perturbations with the observed form [17,18].

The success of optimal growth theory in predicting the roll-streak structure observed in perturbed wall-bounded shear flow prior to transition appeared at first to be persuasive that the explanation for observations of this structure in pretransitional flow was secure. Nevertheless, there remained a lingering doubt. For one thing, there is the regularity of the spacing and amplitude of the roll-streak structure in experiments [19,20], which, as remarked by Townsend [21], is characteristic of modal growth. Then there is the observation that streamwise rolls decay in amplitude if background turbulence levels are sufficiently low, which conforms with the expectation of roll decay associated with the optimal growth predicted by transient growth theory [22,23], while rolls grow downstream in the presence of moderate levels of background turbulence intensity [24], which is incompatible with transient growth and suggestive of an underlying unstable mode.

While the absence of roll-streak instability in an unperturbed wall-bounded shear flow is established, pseudospectral theory [25,26] reveals that a highly non-normal operator, such as that of Navier-Stokes (NS) dynamics linearized about a strongly sheared flow, can be destabilized by small perturbations to the dynamical operator itself. Consistently, it was recently shown that an emergent instability with roll-streak structure arises from interaction between this structure and a field of background turbulence with sufficient amplitude [27]. This instability does not have an analytical expression in the linearized NS dynamics of the laminar flow because it is not a linear instability of the laminar shear flow but instead arises from systematic organization by the roll-streak structure of the Reynolds stress associated with the incoherent background turbulence. The analytical expression of this instability therefore exists only in the equations for the associated statistical state dynamics (SSD). The formulation of SSD used in this work to study this instability, referred to as S3T, is a second-order closure of the Navier-Stokes dynamics in which full nonlinearity is retained in the streamwise mean equation (first cumulant) while the dynamics of the perturbation covariance (second cumulant) is linearized about the instantaneous streamwise mean flow. Nonlinear interaction occurs between the mean flow dynamics (defined as flow components with streamwise wave number $k_x = 0$) and the perturbation covariance obtained from flow components with streamwise wave number $k_x \neq 0$, while nonlinearity is parametrized by a stochastic excitation in the perturbation dynamics rather than being explicitly calculated. This quasilinear formulation in which nonlinearity is parametrized in the perturbation dynamics has necessarily the dynamical structure of a second order closure of the NS as noted by Herring [28]. We refer to this dynamical restriction of the full NS equations as RNL. We employ the RNL restriction in constructing finite ensemble approximations of the equivalently infinite ensemble S3T. Consistent with this usage, the perturbation equations

making up the ensemble in an RNL-based approximation to S3T are used only to calculate an approximate covariance. As a consequence, phase information is not retained for the perturbation fields, only their second-order correlations being relevant to a second-order SSD.

As alluded to above, the approximation to the perturbation covariance obtained using RNL dynamics can be systematically improved by forming a mean covariance from an ensemble of RNL perturbation equations sharing a single mean flow. In the case that an N-member ensemble is used to approximate the covariance, the SSD approximation is referred to as RNL_N [29]. In the limit $N \to \infty$, S3T dynamics is recovered. The RNL approximation has the advantage that it can be easily implemented at high resolution. Moreover, simulations made using the RNL approximation can be compared to the same DNS implementation that was restricted to obtain the RNL system [11,30].

Further insight can be obtained by proceeding similarly with the NS equations by formally separating the full dynamics into mean and perturbation equations and then calculating an ensemble-average second-order closure using an N-member ensemble of perturbation equations sharing a single mean flow in a manner parallel to the method used in constructing RNL_N but retaining full nonlinearity in the individual perturbation equations of the ensemble. This closure, which will be referred to as NL_N, corresponds to a complete cumulant expansion of the SSD solved up to second order. We find that in our example problem satisfactory convergence of RNL_N and NL_N is obtained for N as small as 10.

Consider a Couette flow subjected to a random excitation that is statistically streamwise and spanwise homogeneous and has zero mean with respect to time and space averaging. The S3T system predicts a bifurcation occurring at a critical amplitude of the excitation in which an unstable roll-streak structure emerges as an instability of the S3T dynamics. It is important at this point to be clear about what entity is being referred to as unstable. The unstable mode we are studying arises as an eigenmode with roll-streak structure at infinitesimal amplitude that eventually grows sufficiently to become a nonlinearly equilibrated finite-amplitude equilibrium that retains roll-streak structure. The existence of coherent roll-streak structures in the flow is therefore explained by the growth and equilibration of this unstable mode. It is perhaps more correct to say that the flow is unstable to this roll-streak structure than to say that this roll-streak structure is unstable, which would admit the alternative interpretation that the finite-amplitude roll-streak structure is itself unstable. At sufficiently high background turbulence levels the finite-amplitude roll-streak structure proceeding from the S3T unstable mode does become itself subject to secondary instability leading to transition to a self-sustaining turbulent state as we will show. The perturbative S3T instability connects directly to the finite-amplitude roll-streak structure, which becomes secondarily unstable, but these secondary instabilities are not of roll-streak form. There is an analogy between equilibrated finite-amplitude roll-streak structures in S3T and exact coherent structures in laminar flow [31–36], although exact coherent structures are finite-amplitude isolated equilibria that do not connect to linear instabilities of the spanwise independent laminar flow as the S3T roll-streak structures connect to their associated S3T unstable modes. While S3T finite-amplitude roll-streak structures become secondarily unstable only when these roll-streak structures reach high amplitude under excitation by strong background turbulence, the isolated exact coherent structures generally support secondary instabilities, for example, those discussed by Deguchi and Hall [36,37] in their investigation of the stability of the finite-amplitude states in vortex-wave interaction theory. We remark that once its secondary instability becomes supported the coherent roll-streak S3T equilibrium is rapidly destroyed. This observation suggests that physically realistic levels of background turbulence should excite the parasitic modes of exact coherent structures as well. In order to maintain such unstable structures it is necessary to suppress naturally occurring sources of perturbations that would necessarily excite the parasitic modes to which these structures are vulnerable. In contrast, the S3T instability results from organization of the background disturbances that constitutes its energy source, so rather than being detrimental to it, the S3T mode growth rate and amplitude at equilibrium increases with increasing background disturbance amplitude.

Returning now to the S3T instabilities with roll-streak form, as the background turbulence excitation is increased, at first the streamwise and spanwise averaged mean flow differs little from the laminar Couette profile while superimposed on this profile is a fixed-point finite-amplitude

roll-streak structure. With a further increase in the excitation amplitude another critical value is exceeded at which the flow transitions to turbulence. The existence of these three statistical regimes under increasing levels of background turbulence—the near laminar state, the near laminar with superimposed finite-amplitude equilibrated roll-streak structure, and the turbulent regime characterized by chaotic fluctuation of the roll-streak structure in Couette flow—was predicted using S3T [27]. The purpose of this paper is to determine whether these predictions made using S3T are reflected in ensemble RNL and NL SSD approximations and to analyze the convergence to the S3T predictions obtained using the RNL_N and NL_N approximations as $N \to \infty$.

II. FORMULATION OF THE S3T SYSTEM

Consider a plane Couette flow with streamwise direction x, wall-normal direction y, and spanwise direction z in which background turbulence is maintained by stochastic excitation applied throughout the flow. The lengths of the channel in the streamwise, wall-normal, and spanwise directions are, respectively, L_x, $2h$, and L_z. The channel walls are at $y/h = -1$ and 1. Spatial and temporal averages are denoted by square brackets with a subscript denoting the independent variable over which the average is taken, i.e., spanwise averages by $[\cdot]_z = L_z^{-1} \int_0^{L_z} \cdot \, dz$ and time averages by $[\cdot]_t = T^{-1} \int_0^T \cdot \, dt$, with T sufficiently long. Multiple subscripts denote an average over the subscripted variables in the order they appear, i.e., $[\cdot]_{x,y} \stackrel{\text{def}}{=} [[\cdot]_x]_y$. The vector velocity $\mathbf{u}$ is decomposed into its streamwise mean, denoted by $\mathbf{U}(y,z,t) \stackrel{\text{def}}{=} [\mathbf{u}(x,y,z,t)]_x$, and the deviation from this mean (the perturbation), denoted by $\mathbf{u}'(x,y,z,t)$, so that $\mathbf{u} = \mathbf{U} + \mathbf{u}'$. The pressure is similarly decomposed as $p = P(y,z,t) + p'(x,y,z,t)$. Velocity is nondimensionalized by the velocity at the wall U_w at $y/h = 1$, lengths by h, and time by h/U_w. The nondimensional NS equations decomposed into an equation for the mean and an equation for the perturbation are

$$\partial_t \mathbf{U} + \mathbf{U} \cdot \nabla \mathbf{U} + \nabla P - \Delta \mathbf{U}/\mathrm{Re} = -[\mathbf{u}' \cdot \nabla \mathbf{u}']_x, \tag{1a}$$

$$\partial_t \mathbf{u}' + \mathbf{U} \cdot \nabla \mathbf{u}' + \mathbf{u}' \cdot \nabla \mathbf{U} + \nabla p' - \Delta \mathbf{u}'/\mathrm{Re} = -\mathbf{u}' \cdot \nabla \mathbf{u}' + [\mathbf{u}' \cdot \nabla \mathbf{u}']_x + \sqrt{\varepsilon}\, \mathbf{f}', \tag{1b}$$

$$\nabla \cdot \mathbf{U} = 0, \quad \nabla \cdot \mathbf{u}' = 0, \quad \nabla \cdot \mathbf{f}' = 0, \tag{1c}$$

where $\mathrm{Re} = U_w h/\nu$ is the Reynolds number. The velocities and the stochastic excitation $\mathbf{f}'(x,y,z,t)$ satisfy periodic boundary conditions in the z and x directions and no-slip boundary conditions in the cross-stream direction: $\mathbf{U}(x,\pm 1,z,t) = (\pm 1,0,0)$ and $\mathbf{u}'(x,\pm 1,z,t) = \mathbf{f}'(x,\pm 1,z,t) = 0$. The stochastic excitation is applied only to the streamwise varying Fourier components of the flow. It is nondivergent, has zero ensemble mean $\langle \mathbf{f}' \rangle = 0$ (the ensemble mean over excitation realizations being denoted by $\langle \cdot \rangle$), and is δ-correlated in time and statistically homogeneous in the x and z directions. δ-correlation in time of the excitations implies that the energy input by the stochastic excitation is independent of the flow state and can be parametrized by ε in Eq. (1b). The x,y,z components of $\mathbf{U}$ are (U,V,W) and the corresponding components of $\mathbf{u}'$ are (u',v',w'). The streak component of the streamwise mean flow is denoted by U_s and is defined as

$$U_s \stackrel{\text{def}}{=} U - [U]_z. \tag{2}$$

The streamwise mean cross-stream and spanwise velocities V and W, respectively, are found to primarily constitute the roll vortices. We also define the streak energy density $E_s = [U_s^2/2]_{y,z}$, the roll energy density $E_r = [(V^2 + W^2)/2]_{y,z}$, and the perturbation energy density $E_p = [|\mathbf{u}'|^2/2]_{x,y,z}$. Energy is injected from the moving walls at rate $I = (2\,\mathrm{Re})^{-1}[\partial_y U|_{y=1} + \partial_y U|_{y=-1}]_z$ and at rate ε from the appropriately normalized stochastic forcing. Energy is dissipated at rate $D = \mathrm{Re}^{-1}[|\nabla \times \mathbf{u}|^2]_{x,y,z}$. By I_c and D_c we denote the energy injection and dissipation rates of the Couette flow, respectively.

The S3T dynamics is an SSD governing the evolution of the first two cumulants consisting of the streamwise mean flow $\mathbf{U} = (U,V,W)$ or $\mathbf{U} = (U_x,U_y,U_z)$ and the second cumulants that are the

same time covariances of the Fourier components of the velocity fluctuations $\hat{u}'_{\alpha,k_x}$, where the index $\alpha = x, y, z$ indicates the velocity component in the Fourier expansion of the perturbation velocity $\mathbf{u}'$,

$$\mathbf{u}'(x,y,z,t) = \sum_{k_x > 0} \Re\left[\hat{\mathbf{u}}'_{k_x}(y,z,t)e^{ik_x x}\right], \tag{3}$$

with k_x the streamwise wave numbers that are excited by the stochastic excitation ($\Re$ denotes the real part). We similarly expand the excitation in its Fourier components $\hat{\mathbf{f}}'_{k_x}$. In this study we limit the stochastic excitation to only the streamwise fundamental wave number $k_x = 2\pi/L_x$ and, as a result, the subscript k_x in the velocity and excitation components can be dropped without ambiguity. Because in the S3T equations the perturbation-perturbation interactions are not included, this choice of excitation implies that the S3T flow field perturbations have power only at the streamwise component that is forced. The covariance variables of S3T are the covariances of the velocity components of Fourier component k_x between point $1 \overset{\text{def}}{=} (y_1, z_2)$ and point $2 \overset{\text{def}}{=} (y_2, z_2)$ evaluated at the same time:

$$C_{\alpha\beta}(1,2) = \langle \hat{u}'_\alpha(1)\hat{u}'^*_\beta(2) \rangle, \tag{4}$$

which is a function of the coordinates of the two points (1) and (2) on the (y,z) plane and of time ($*$ denotes complex conjugation). The S3T equations are

$$\partial_t U_\alpha + U_\beta \partial_\beta U_\alpha + \partial_\alpha P - \Delta U_\alpha/\mathrm{Re} = -\tfrac{1}{2}\Re[\partial_y C_{y\alpha}(1,1) + \partial_z C_{z\alpha}(1,1)], \tag{5a}$$

$$\partial_t C_{\alpha\beta}(1,2) = A_{\alpha\gamma}(1)C_{\gamma\beta}(1,2) + A^*_{\beta\gamma}(2)C_{\alpha\gamma}(1,2) + Q_{\alpha\beta}(1,2), \tag{5b}$$

$$\partial_a U_a = 0, \hat{\partial}_\alpha(1)C_{\alpha\beta}(1,2) = \hat{\partial}^*_\beta(2)C_{\alpha\beta}(1,2) = 0, \tag{5c}$$

with summation convention on repeated indices and the operator $\hat{\partial} \overset{\text{def}}{=} (ik_x, \partial_y, \partial_z)$ (for a derivation see [27]). The operator $A_{\alpha\beta}(1)$ [or $A_{\alpha\beta}(2)$] is the operator governing the quasilinear evolution of streamwise varying perturbations in Eq. (1b) with streamwise wave number $k_x = 2\pi/L_x$ linearized about the instantaneous streamwise mean flow $\mathbf{U}(1)$ [or $\mathbf{U}(2)$] and 1 (or 2) indicates that the operator acts on the 1 (or the 2) variable of $C(1,2)$. Here $Q_{\alpha\beta}(1,2)$ are the spatial covariances of the k_x Fourier components of the forcing components $\hat{f}_i$ and are defined as

$$\langle \hat{f}_\alpha(1,t_1)\hat{f}^*_\beta(2,t_2) \rangle = \delta(t_1 - t_2)Q_{\alpha\beta}(1,2). \tag{6}$$

Using S3T we can find roll-streak structures that are independent of time because their forcing derives from a converged covariance obtained from an equivalently infinite ensemble of independent realizations. These fixed-point equilibria are imperfectly reflected in individual realizations because fluctuations in the covariance arise due to the finiteness of the equivalent ensemble of statistically independent structures that fit in the channel. These fluctuations in the covariance result in imperfect correspondence with the underlying equilibrium structure revealed by S3T (see [38,39]). In order to verify that the S3T fixed point does in fact underly the dynamics of the roll-streak structure observed in RNL and NS simulations it is useful to obtain solutions lying on the continuum from the single-realization solution to the infinite-ensemble S3T fixed-point solution. The S3T dynamics is approached by RNL_N simulations as $N \to \infty$. The RNL_N system is governed by the system of equations

$$\partial_t \mathbf{U} + \mathbf{U} \cdot \nabla \mathbf{U} + \nabla P - \Delta \mathbf{U}/\mathrm{Re} = -\langle [\mathbf{u}' \cdot \nabla \mathbf{u}']_x \rangle_N, \tag{7a}$$

$$\partial_t \mathbf{u}'_n + \mathbf{U} \cdot \nabla \mathbf{u}'_n + \mathbf{u}'_n \cdot \nabla \mathbf{U} + \nabla p'_n - \Delta \mathbf{u}'_n/\mathrm{Re} = \sqrt{\varepsilon}\,\mathbf{f}'_n, \tag{7b}$$

$$\nabla \cdot \mathbf{U} = 0, \quad \nabla \cdot \mathbf{u}'_n = 0, \quad \nabla \cdot \mathbf{f}'_n = 0, \tag{7c}$$

where $n = 1, \ldots, N$ indicates the ensemble member and $\langle \cdot \rangle_N$ indicates an average over the N ensemble members. Note that as required by correspondence with S3T dynamics, the perturbation-perturbation interaction in Eq. (1b) is ignored.

In a similar manner we can form ensemble NL_N equations

$$\partial_t \mathbf{U} + \mathbf{U} \cdot \boldsymbol{\nabla} \mathbf{U} + \boldsymbol{\nabla} P - \Delta \mathbf{U}/\mathrm{Re} = -\langle[\mathbf{u}' \cdot \boldsymbol{\nabla}\mathbf{u}']_x\rangle_N, \tag{8a}$$

$$\partial_t \mathbf{u}'_n + \mathbf{U} \cdot \boldsymbol{\nabla}\mathbf{u}'_n + \mathbf{u}'_n \cdot \boldsymbol{\nabla}\mathbf{U} + \boldsymbol{\nabla} p'_n - \Delta\mathbf{u}'_n/\mathrm{Re} = -\mathbf{u}'_n \cdot \boldsymbol{\nabla}\mathbf{u}'_n + [\mathbf{u}'_n \cdot \boldsymbol{\nabla}\mathbf{u}'_n]_x + \sqrt{\varepsilon}\,\mathbf{f}'_n, \tag{8b}$$

$$\boldsymbol{\nabla} \cdot \mathbf{U} = 0, \quad \boldsymbol{\nabla} \cdot \mathbf{u}'_n = 0, \quad \boldsymbol{\nabla} \cdot \mathbf{f}'_n = 0. \tag{8c}$$

We are interested in whether the analytical predictions of the S3T equations are approached in RNL_N and NL_N simulations as N increases. Results are presented for the minimal Couette flow channel of Hamilton *et al.* [7] at $R = 400$ (based on channel half-width) with streamwise length $L_x = 1.75\pi$, spanwise length $L_z = 1.2\pi$, and channel half-width $L_y = 1$. The gravest streamwise wave number $k_x = 2\pi/L_x$ is stochastically excited using independent compact support cross-stream velocity and cross-stream vorticity structures in (y, z). Numerical calculations employ $N_y = 21$ grid points in the cross-stream direction and 32 harmonics in the spanwise and streamwise directions. Other stochastic excitations produce only qualitative differences in the results. A study of the S3T dynamics of this channel model was reported in Ref. [27].

III. COMPARISON OF ROLL-STREAK EMERGENCE AND EQUILIBRATION IN S3T, RNL_N, AND NL_N

The S3T system (5) supports spanwise uniform fixed-point solutions with streamwise mean flow form $\mathbf{U}_e = (U_e(y), 0, 0)$ and associated spanwise covariance $C_e(y_1, y_2, z_1 - z_2)$. Taking $\varepsilon = 0$ recovers the laminar Couette flow $U_e = y$ with $C_e = 0$. As ε increases the equilibrium streamwise mean flow $U_e(y)$ departs from the Couette flow. Stability of these spanwise uniform S3T equilibria can be determined as a function of ε using the S3T equations (5) linearized about these fixed points [27].

Eigenvalues and the associated mean flow eigenfunction structure for the first two most unstable S3T modes are shown in Fig. 1. The complete associated eigenfunctions comprise both a mean flow component $(\delta U(y, z), \delta V(y, z), \delta W(y, z))$, which is shown in Fig. 1, and a covariance component $\delta C(y_1, y_2, z_1, z_2)$. The structure of the mean flow component of these eigenfunctions changes only slightly as the amplitude of the forcing ε increases. The eigenfunctions consist of low- and high-speed streamwise streaks together with roll circulations exactly collocated to reinforce the streak velocity. Despite being more highly dissipated by diffusion, the mean flow eigenfunction that becomes unstable first as ε increases is not the eigenstructure with the gravest spanwise wave number $k_z = 2\pi/L_z = 1.67$, shown in Fig. 1(b), but the second spanwise harmonic with wave number $k_z = 4\pi/L_z = 3.33$, shown in Fig. 1(a). Destabilization of these roll-streak eigenfunctions can be traced to a universal positive feedback mechanism operating in turbulent flows: When incoherent turbulence is perturbed by a coherent streak, the streak distorts the incoherent turbulence so as to induce ensemble mean Reynolds stresses forcing streamwise mean roll circulations configured to reinforce the streak perturbation that gave rise to them (see [27]). The modal streak perturbations of the fastest growing eigenfunctions induce the strongest such feedback (when account has been taken for viscous damping).

We note that neutral mode and critical layer based self-sustaining process (SSP) theories such as the vortex-wave interaction (VWI) theory predict structures at variance with the S3T unstable modes we obtain. As shown in Figs. 1(a) and 1(b), organization of the Reynolds stress by the streak (even at perturbational amplitude) results in a smooth domainwide forcing of the roll circulation. At high Reynolds number in the neutral mode SSP and VWI mechanisms this interaction is localized at the critical layer [32,34,36,40]. The interaction between perturbations and mean flow in neutral mode and VWI theories by necessity occurs near the the critical layer in the inviscid limit because according to the nonacceleration theorem at steady state and in the absence of forcing and dissipation there is no interaction between mean and perturbations except at the critical layer [41–43]. In S3T there is forcing and consequently the interaction is not required to be concentrated in the vicinity
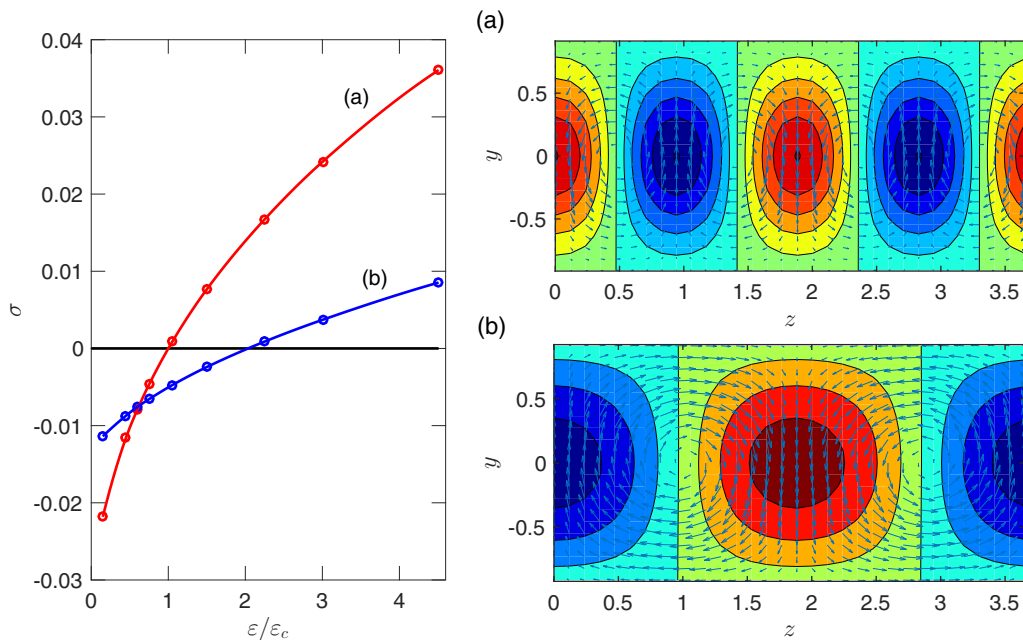
FIG. 1. Shown on the left is the growth rate of the two most unstable S3T eigenfunctions about the spanwise homogeneous S3T equilibrium as a function of the excitation amplitude of the background turbulence ε. On the right is the structure of the corresponding eigenfunctions with growth rate (a) and (b) for excitation amplitude $\varepsilon/\varepsilon_c = 2$. Shown are contours of the streak velocity U_s and velocity vectors of the components (V, W) plotted on a (y, z) plane cross section. The structure of these eigenfunctions does not change appreciably for $\varepsilon/\varepsilon_c < 6$. At $\varepsilon = \varepsilon_c$ the S3T spanwise uniform equilibrium bifurcates to a finite-amplitude equilibrium with perturbation structure close to that of the most unstable eigenfunction shown in (a). The channel is minimal with $L_x = 1.75\pi$ and $L_z = 1.2\pi$, the Reynolds number is Re $= 400$, and the stochastic forcing excites only Fourier components with streamwise wave number $k_x = 2\pi/L_z = 1.143$. The critical ε_c sustains a background turbulent field with mean energy 0.14% of the Couette flow energy.

of the critical layer even in the inviscid limit. The modes we calculate organize distributions of Reynolds stress with divergence exactly coherent with the mode roll structure, as is required of a mode solution, and not in any sense concentrated at a critical surface. In fact, the lack of any evidence for concentration of Reynolds stress divergence at a particular cross-stream location either in our stable roll-streak regime or in our self-sustaining turbulence simulations argues against a mechanism relying on an interaction localized at a critical surface.

Stability analysis of the spanwise homogeneous equilibrium of the S3T system determines the critical excitation ε_c at which this turbulent equilibrium state becomes unstable. For the parameters of our example problem this ε_c corresponds to maintaining in the Couette flow a perturbation field with mean energy density 0.14% of the energy density of the Couette flow. For $\varepsilon > \varepsilon_c$ the spanwise symmetry is broken with the emergence of mean flow structures in the form of the fastest growing eigenfunction that is shown in Fig. 1(a). Over a finite interval $\varepsilon_c < \varepsilon < \varepsilon_t$ the unstable S3T eigenfunction equilibrates nonlinearly to form new finite-amplitude S3T equilibria with roll-streak structure qualitatively similar to the corresponding eigenfunction (for our examples $\varepsilon_t/\varepsilon_c \approx 5.5$).

A bifurcation diagram showing the maximum of the streak velocity U_s and of the streamwise mean cross-stream velocity V is shown as a function of ϵ in Fig. 2. The indicated critical ε_c was determined by stability analysis of the S3T system. For $\varepsilon/\varepsilon_c < 1$ the equilibrium is spanwise independent with no coherent roll-streak structure. The equilibrium values shown in Fig. 2 were
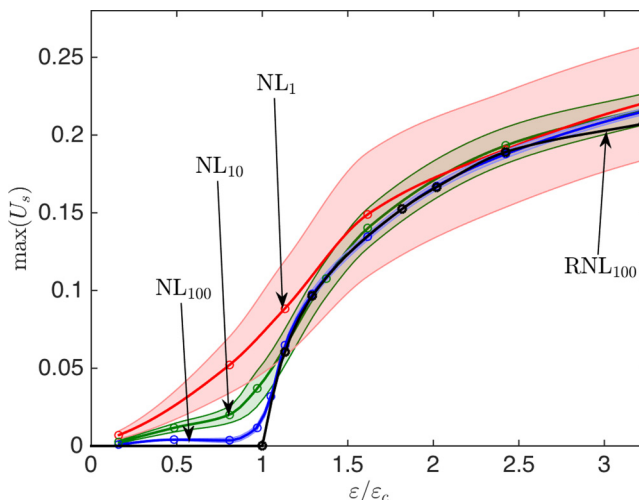
FIG. 2. Bifurcation diagram for the Couette problem. Shown is the time mean of the maximum value of the streak amplitude U_s as a function of the stochastic excitation amplitude ε for an NL_1 simulation (red curve), an ensemble NL_{10} simulation (green curve), an ensemble NL_{100} simulation (blue curve), and an ensemble RNL_{100} simulation (black curve). The critical bifurcation value was determined from stability analysis of the S3T system and it has been confirmed that this value is closely approximated using RNL_{100}. For $\varepsilon/\varepsilon_c < 1$, S3T predicts that the streamwise streak and roll amplitude is zero. At $\varepsilon = \varepsilon_c$ the S3T spanwise uniform equilibrium bifurcates, giving rise to a finite-amplitude equilibrium with roll and streak. The NL_1 and NL_{10} simulations exhibit fluctuating streak-roll structures and one standard deviation of the fluctuations corresponds to the shaded regions in the figure. The fluctuations in the ensemble NL_{100} and RNL_{100} simulations are small and only those associated with NL_{100} are shown. Other parameters are as in Fig. 1.

obtained using RNL_{100} simulations. These RNL_{100} equilibria have been verified to be very close to the equivalently infinite-ensemble S3T equilibria.

Single NL and ensemble NL integrations allow us to study the correspondence between the infinite-ensemble predictions of S3T analysis and NL turbulence. While finite-ensemble simulations produce fluctuating roll-streak structures, we find that even in the case of a realization simulation, corresponding to $N = 1$, a clear roll-streak structure emerges for $\varepsilon > \varepsilon_c$ that exhibits great persistence and has the same structure as that predicted by the S3T system. An indicative comparison between an S3T equilibrium roll-streak structure and a snapshot of the corresponding roll-streak from an NL_1 simulation at $\varepsilon/\varepsilon_c = 3$ is shown in Fig. 3.

While the S3T equilibria are fixed points, the corresponding roll-streak structure in the NL_1 simulation reflect the time independence of the S3T equilibria imperfectly. However, it is persuasive that the analytical structure revealed by the S3T system underlies the behavior seen in the NL_1 simulation; for example, see the snapshots shown in Fig. 4. Noise-driven fluctuations of the ensemble structure are also apparent in the bifurcation diagram shown in Fig. 2 in which the mean and variance of the maximum streak U_s in NL_1 and NL_{10} are indicated. The reflection of the analytical S3T bifurcation is clearly seen in the NL_{10} results and near convergence is obtained in the NL_{100} results.

We have demonstrated that the unstable roll-streak modes and associated finite-amplitude S3T equilibria that are revealed by S3T analysis give rise to the structure observed in pretransitional turbulent Couette flow in both NL and ensemble NL simulations. However, the stable S3T modes supported in the S3T stable the interval ($0 < \varepsilon/\varepsilon_c < 1$) are also important structures in the dynamics of pretransitional turbulence. While not excited in the fluctuation-free S3T dynamics, these stable S3T modes are robustly excited by fluctuations in the forcing in NL_1 simulations (see [38,39,45]). Correspondingly, for subcritical excitation ($0 < \varepsilon/\varepsilon_c < 1$) the mean flow of NL or ensemble NL
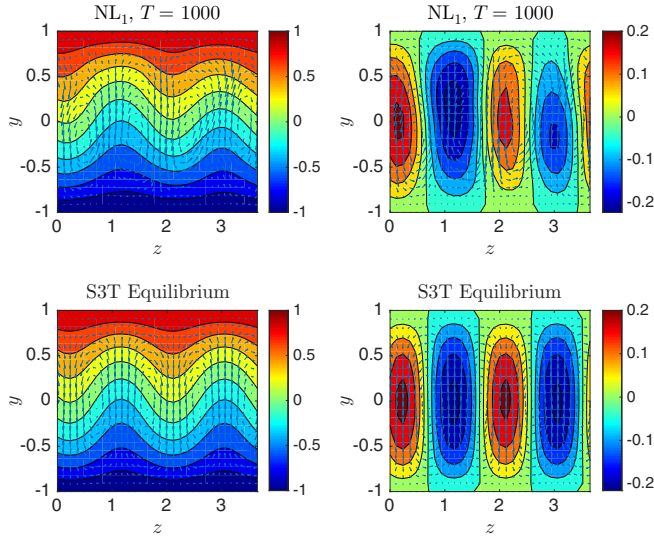
FIG. 3. The top panels show a snapshot of the streamwise mean flow from an NL_1 simulation at stochastic excitation amplitude $\varepsilon/\varepsilon_c = 3$. Shown are contours of the streamwise mean velocity U (top left), streak velocity U_s (top right), and velocity vectors of the components (V, W) in the (y, z) plane at $t = 1000$ of the simulation. The bottom panels show the corresponding streamwise mean flow for the S3T system at $\varepsilon/\varepsilon_c = 3$. This figure shows that the equilibrium roll-streak regime predicted by S3T is reflected in single realizations of the NL equations. The development of the roll-streak structure in an NL_1 simulation can be seen in movie 1 of the Supplemental Material [44]. The development of the roll-streak equilibrium in an S3T equilibrium simulation can be seen in movie 2 in Ref. [44]. Parameters are as in the previous figures.
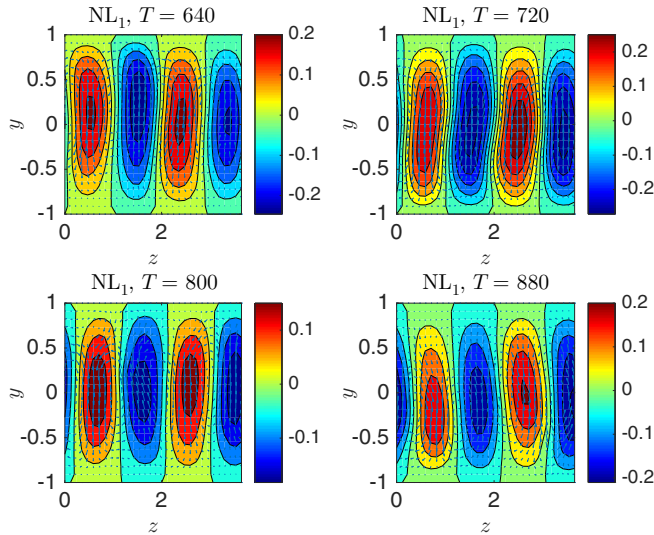

FIG. 4. Snapshots at times $t = 640, 720, 800, 880$ of the contours of the streak velocity U_s and velocity vectors of the components (V, W) plotted on a (y, z) plane cross section from an NL_1 simulation at stochastic excitation amplitude $\varepsilon/\varepsilon_c = 3$. This figure shows the persistence of the organized structure in NL_1. This structure and its persistence stem from the underlying equilibrium state that exists for this excitation amplitude in the S3T dynamics. The other parameters are as in the previous figures.
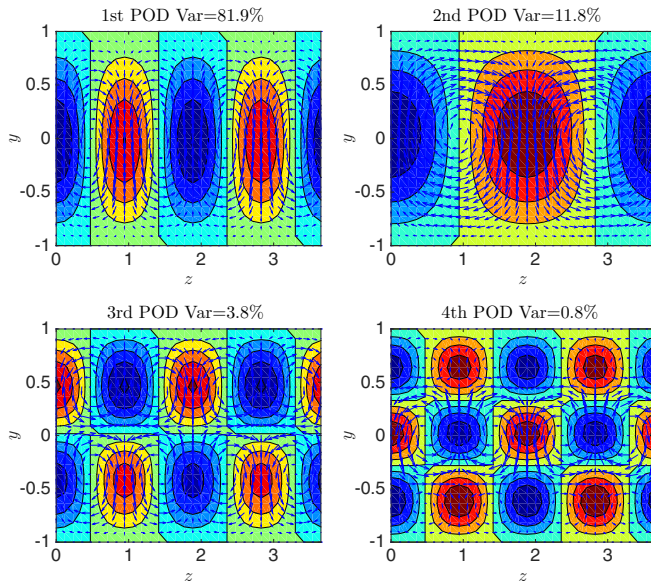
FIG. 5. Contours of streak velocity U_s and vectors of roll components (V, W) plotted on a (y, z) cross section for the first four PODs of the streamwise mean flow fluctuations of an NL_1 forced at $\varepsilon/\varepsilon_c = 0.75$. The PODs come in pairs. The first pair of PODs that account for 82% of the energy of the fluctuations of the streamwise mean flow has the structure of the least damped S3T mode, which because of its more effective energetic interaction with the covariance, as revealed by S3T, is not the least viscously damped mode in the channel. This figure shows that the fluctuations in the NL_1 simulations reveal the S3T stable modes. Other parameters as in the previous figures.

simulations reveals fluctuating (y, z) structure arising from excitation of the stable manifold of S3T eigenmodes. A proper orthogonal decomposition (POD) analysis (see [46]) of the streamwise mean flow verifies that the streamwise mean fluctuations reflect the structure of and are ordered by the damping of the stable eigenmodes identified by S3T analysis (see [47]). For example, the first four PODs of NL_1 at $\varepsilon/\varepsilon_c = 0.75$, shown in Fig. 5, have the structure predicted by the S3T eigenmodes. Consistent with S3T analysis, the first POD corresponds to the mode with spanwise wave number $k_z = 4\pi/L_z$, which corresponds to the least stable eigenfunction at this $\varepsilon/\varepsilon_c$. Note that all PODs exhibit exact alignment of the roll circulations with the streaks. These results are consistent with identifying the POD structures with the eigenmodes predicted by S3T stability analysis. Consistent with these stable modes being excited by turbulent fluctuations, as $\varepsilon/\varepsilon_c \to 1$ fluctuations of roll-streak form exhibit enhanced variance (cf. Fig. 2), which is indicative of approach to a bifurcation and is a phenomenon analogous to that of critical opalescence on approach to a fluid phase transition.

IV. TRANSITION TO TURBULENCE

At background turbulence excitation parameters exceeding ε_t ($\varepsilon_t/\varepsilon_c \approx 5.5$ for the chosen parameters) the finite-amplitude roll-streak equilibria are no longer S3T stable and the flow transitions to a turbulent state, which is self-sustaining and persists even when the background turbulence excitation parameter is subsequently set to $\varepsilon = 0$ (see [27]). RNL_1 and NL_1 also transition to essentially similar self-sustaining turbulence. Example trajectories of transition from the laminar equilibrium state to the turbulent attractor for NL_1 and S3T are shown in Fig. 6.

A typical evolution of the perturbation energy density E_p, streak energy density E_s, and roll energy density E_r of the background turbulence excitation parameter $\varepsilon/\varepsilon_c = 9$ is shown in Fig. 7 for
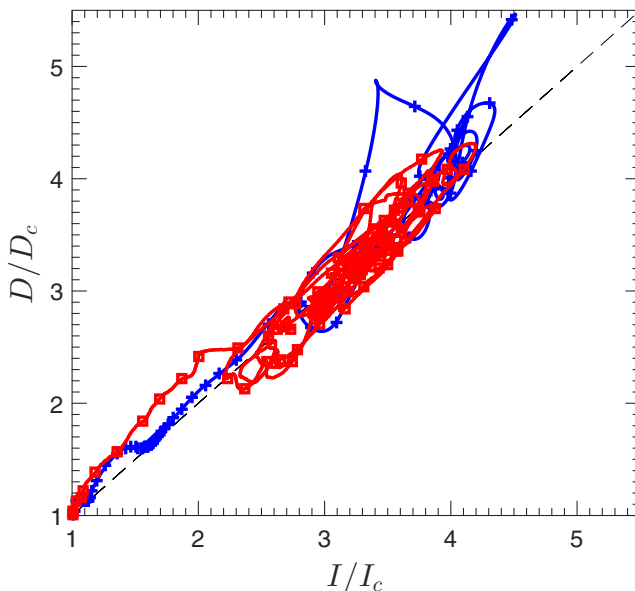
FIG. 6. Evolution of energy input rate I/I_c and dissipation rate D/D_c from the laminar state to the turbulent state in an NL_1 simulation (squares and solid line) and in an S3T simulation (crosses and solid line) with background turbulence excitation parameter $\varepsilon/\varepsilon_c = 9$. Symbols are marking intervals of ten units of time. The metastable state is characterized by $D/D_c \approx 1.7$. The parameters are as in the previous figures.

the case of S3T. The S3T integration was initialized with a small random streak perturbation. The flow transitions to turbulence at time $T \approx 550$. In this transition process the roll-streak emerges at first as an S3T instability that equilibrates by time $T \approx 200$ to the quasiequilibrium finite-amplitude roll-streak structure shown in the left panel of Fig. 8. This quasiequilibrium is associated with
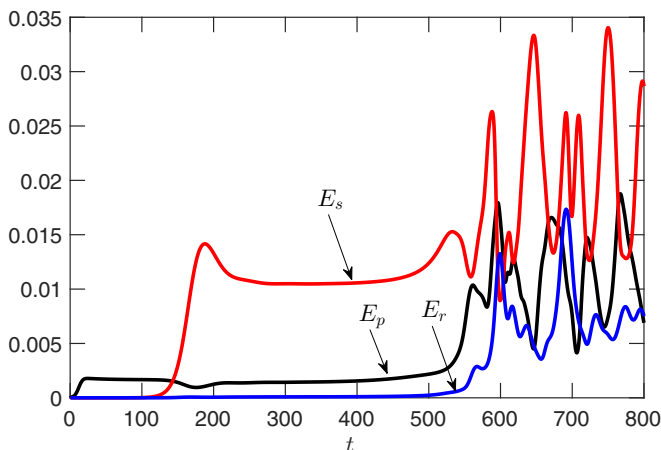

FIG. 7. Evolution of the streak energy E_r, roll energy E_r, and perturbation energy E_p in an S3T integration at $\varepsilon/\varepsilon_c = 9$ under spanwise homogeneous forcing. The flow is initialized with a small random streamwise mean perturbation with spanwise dependence in order to break spanwise symmetry. The spanwise symmetric S3T equilibrium is unstable and a quasisteady state emerges by time $t = 200$ with the roll-streak structure shown in Fig. 8. At this supercriticality the roll-streak structure (cf. Fig. 9) is an unstable fixed point of the S3T dynamics and the flow transitions to the turbulent state. Other parameters are as in the previous figures.
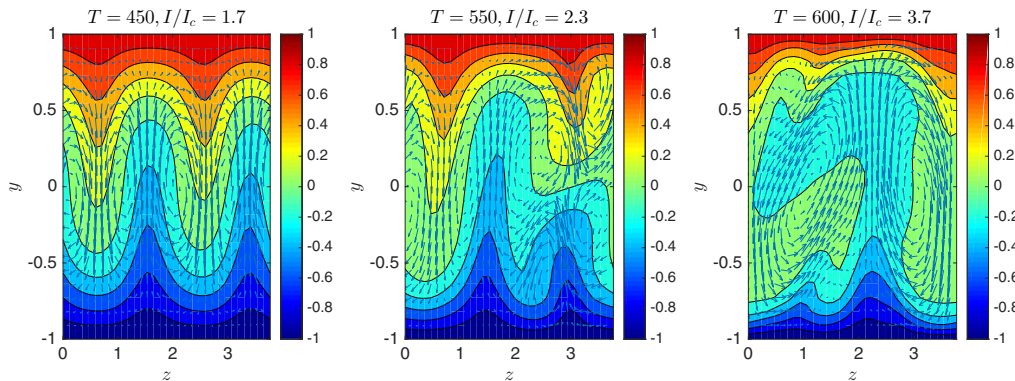
FIG. 8. Snapshots of the streamwise mean flow as it undergoes S3T transition to turbulence under stochastic excitation. Shown are contours of the streak velocity U_s and velocity vectors of the components (V, W) plotted on the (y, z) plane. A quasisteady roll-streak structure forms initially (left panel) with input energy rate $I/I_c \approx 1.7$ and structure near that of the fastest growing S3T instability (cf. Fig. 1), which has spanwise wave number $k_z = 4\pi/L_z$. At about $t = 550$ the flow transitions through initially nearly periodic oscillations to a turbulent roll-streak structure dominated by spanwise wave number one $(k_z = 2\pi/L_z)$. The transition period can be extended by enforcing the mirror symmetry of the streak-roll structure about the streak maximum. Note that after transition the spanwise wave number of the roll-streak structure is half that of the S3T instability. Other parameters are as in the previous figures.

an energy input rate $I/I_c \approx 1.7$, which lies approximately midway between the value associated with the laminar state and that associated with the statistical mean of the turbulent state. At these parameters there exists near this quasiequilibrium a symmetric unstable equilibrium, shown in Fig. 9, which can be converged to by suppressing spanwise asymmetries. In the presence of realistic spanwise asymmetric perturbations excitation of the unstable directions of this equilibrium at about $T \approx 550$ initiates the transition to turbulence. While this pathway to turbulence is typical in all
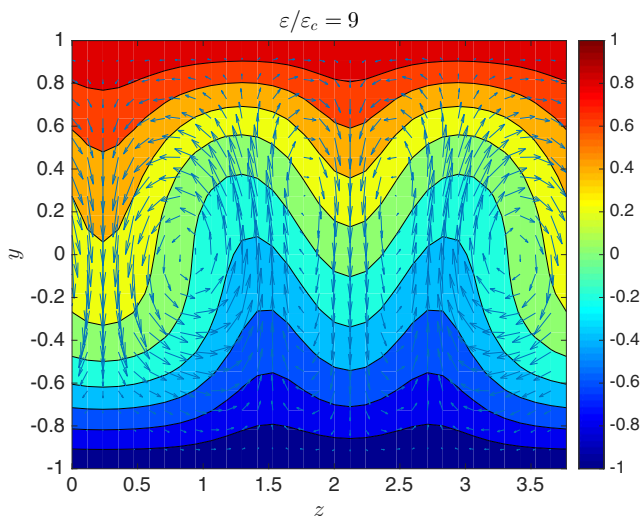

FIG. 9. Unstable roll-streak S3T equilibrium at $\varepsilon/\varepsilon_c = 9$. Shown are contours of the streak velocity U_s and velocity vectors of the components (V, W) plotted on a (y, z) plane cross section. Other parameters are as in the previous figures.
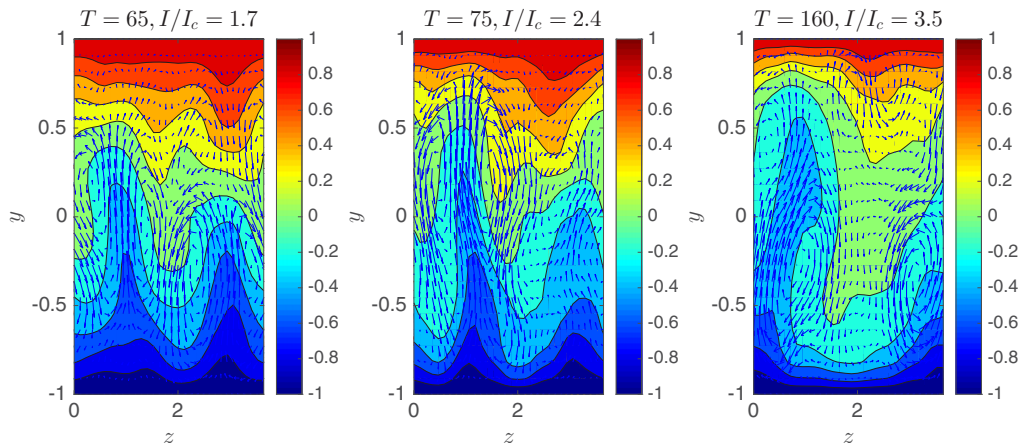
FIG. 10. Snapshots of the streamwise mean flow as it undergoes transition to turbulence in an NL_1 simulation under stochastic excitation with $\varepsilon/\varepsilon_c = 9$. Shown are contours of the streak velocity U_s and velocity vectors of the components (V, W) in the (y, z) plane. The quasisteady roll-streak structure that initially forms, breaks down and the flow transitions to turbulence. The transition is as in the S3T simulation (cf. Figs. 7 and 8), except that the flow passes through the metastable state rapidly. Other parameters are as in the previous figures.

S3T simulations with $\varepsilon > \varepsilon_t$, the timing of transition depends on the structure of the initialized state, which determines the projection on the instability of the S3T unstable equilibrium state. For example, if the flow at $\varepsilon/\varepsilon_c = 9$ is constrained to have no perturbations breaking mirror symmetry in the spanwise direction the flow is attracted to the unstable roll-streak structure shown in Fig. 9 without ever transitioning to turbulence, while if the initial flow state includes a rich spectrum of mirror asymmetric perturbations transition to turbulence occurs rapidly.

This sequence of events, with rapid breakdown of the finite-amplitude roll-streak structure, is observed in NL_1 simulations at $\varepsilon/\varepsilon_c = 9$ when the simulation is initialized with the laminar state. The roll-streak structure associated with the underlying S3T instability arises at first, as in the S3T simulation, but then rapidly transitions to the turbulent state. Snapshots of the roll-streak structure during this transition, which occurs by $T = 90$, are shown in Fig. 10.

V. CONCLUSION

Statistical state dynamics makes available to analysis the manifold of instabilities associated with the systematic organization of the background turbulence by coherent structures. In this work the S3T implementation of SSD was used to study instabilities of this type and their nonlinear extensions in a minimal channel configuration of Couette flow. At first a manifold of stable modes with roll-streak form is supported as the parameter controlling the background turbulence intensity, ε is increased from zero. The least stable mode of this manifold is destabilized at a critical excitation, designated ε_c, and a finite-amplitude stable fixed point with roll-streak structure arises for excitations between ε_c and a second critical value for which the finite-amplitude roll-streak equilibrium is destabilized, designated ε_t. For excitation exceeding ε_t the roll-streak equilibrium is unstable to spanwise asymmetric perturbations and becomes time dependent, resulting in the establishment of the turbulent state with spanwise wave number approximately half that of the equilibrium state. Emergence of finite amplitude roll-streak structure through S3T instability and the subsequent secondary instability provides a new route to turbulence in wall bounded shear flow. In order to study SSD dynamics in more detail we compared S3T to ensemble implementations of a quasilinear model sharing the dynamical restrictions of S3T (RNL_N) and the associated nonlinear model (NL_N). Although the SSD instabilities and their associated fixed-point nonlinear equilibria

and time-dependent statistical mean attractor states have analytical expression only in the S3T implementation of SSD dynamics, the predicted dynamics is clearly reflected in both the dynamically similar quasilinear system (RNL_1) and DNS (NL_1). This correspondence was further examined using ensemble implementations of the RNL and DNS systems. As a consequence of sharing the same dynamical restrictions, the RNL_N system converges to S3T as $N \rightarrow \infty$. Remarkably, the NL_N system, which corresponds to a full closure for this problem, also converges to close correspondence with S3T as $N \rightarrow \infty$. This convergence is reflected in similar bifurcation behavior as well as similar equilibrium structures for the stable fixed-point equilibria. As previously remarked, S3T also predicts a second bifurcation at a higher value of the turbulent excitation parameter that results in destabilization of the finite-amplitude roll-streak equilibria and establishment of a turbulent state corresponding to minimal channel turbulence. Comparison with NL_1 simulations reveals that this mechanism is responsible for bypass transition instigated by background turbulence rather than by an optimal perturbation imposed at sufficiently high amplitude.

---

[1] P. S. Klebanoff, K. D. Tidstrom, and L. M. Sargent, The three-dimensional nature of boundary-layer instability, J. Fluid Mech. **12**, 1 (1962).

[2] S. J. Kline, W. C. Reynolds, F. A. Schraub, and P. W. Runstadler, The structure of turbulent boundary layers, J. Fluid Mech. **30**, 741 (1967).

[3] H. P. Bakewell, Jr. and L. Lumley, Viscous sublayer and adjacent wall region in turbulent pipe flow, Phys. Fluids **10**, 1880 (1967).

[4] J. Kim, S. J. Kline, and W. C. Reynolds, The production of turbulence near a smooth wall in a turbulent boundary layers, J. Fluid Mech. **50**, 133 (1971).

[5] J. Kim, P. Moin, and R. Moser, Turbulence statistics in fully developed channel flow at low Reynolds number, J. Fluid Mech. **177**, 133 (1987).

[6] J. Jiménez and P. Moin, The minimal flow unit in near-wall turbulence, J. Fluid Mech. **225**, 213 (1991).

[7] K. Hamilton, J. Kim, and F. Waleffe, Regeneration mechanisms of near-wall turbulence structures, J. Fluid Mech. **287**, 317 (1995).

[8] W. Schoppa and F. Hussain, Coherent structure generation in near-wall turbulence, J. Fluid Mech. **453**, 57 (2002).

[9] J. Jiménez, Near-wall turbulence, Phys. Fluids **25**, 101302 (2013).

[10] Y. Hwang and C. Cossu, Self-sustained processes in the logarithmic layer of turbulent channel flows, Phys. Fluids **23**, 061702 (2011).

[11] B. F. Farrell, P. J. Ioannou, J. Jiménez, N. C. Constantinou, A. Lozano-Durán, and M.-A. Nikolaidis, A statistical state dynamics-based study of the structure and mechanism of large-scale motions in plane Poiseuille flow, J. Fluid Mech. **809**, 290 (2016).

[12] T. Ellingsen and E. Palm, Stability of linear flow, Phys. Fluids **18**, 487 (1975).

[13] M. T. Landahl, A note on an algebraic instability of inviscid parallel shear flows, J. Fluid Mech. **98**, 243 (1980).

[14] B. F. Farrell and P. J. Ioannou, Generalized stability. Part I: Autonomous operators, J. Atmos. Sci. **53**, 2025 (1996).

[15] B. F. Farrell and P. J. Ioannou, Generalized stability. Part II: Non-autonomous operators, J. Atmos. Sci. **53**, 2041 (1996).

[16] P. J. Schmid and D. S. Henningson, *Stability and Transition in Shear Flows* (Springer, New York, 2001).

[17] K. M. Butler and B. F. Farrell, Three-dimensional optimal perturbations in viscous shear flows, Phys. Fluids **4**, 1637 (1992).

[18] S. C. Reddy and D. S. Henningson, Energy growth in viscous channel flows, J. Fluid Mech. **252**, 209 (1993).

[19] M. R. Head and I. Rechenberg, The Preston tube as a means of measuring skin friction, J. Fluid Mech. **14**, 1 (1962).

[20] P. Bradshaw, The effect of wind-tunnel screens on nominally two-dimensional boundary layers, J. Fluid Mech. **22**, 679 (1965).

[21] A. A. Townsend, *The Structure of Turbulent Shear Flow*, 2nd ed. (Cambridge University Press, Cambridge, 1976).

[22] P. H. Alfredsson and M. Matsubara, in *Proceedings of the Transitional Boundary Layers in Aeronautics*, edited by R. A. W. M. Henkes and J. L. van Ingen (Elsevier Science, Amsterdam, 1996), p. 373.

[23] K. J. A. Westin, A. A. Bakchinov, V. V. Kozlov, and P. H. Alfredsson, Experiments on localized disturbances in a flat plate boundary layer. Part 1. The receptivity and evolution of a localized free stream disturbance, Eur. J. Mech. B **17**, 823 (1998).

[24] K. J. A. Westin, A. V. Boiko, B. G. B. Klingmann, V. V. Kozlov, and P. H. Alfredsson, Experiments in a boundary layer subjected to free stream turbulence. Part 1. Boundary layer structure and receptivity, J. Fluid Mech. **281**, 193 (1994).

[25] L. N. Trefethen, A. E. Trefethen, S. C. Reddy, and T. A. Driscoll, Hydrodynamic stability without eigenvalues, Science **261**, 578 (1993).

[26] L. N. Trefethen and M. Embree, *Spectra and Pseudospectra: The Behavior of Nonnormal Matrices and Operators* (Princeton University Press, Princeton, 2005).

[27] B. F. Farrell and P. J. Ioannou, Dynamics of streamwise rolls and streaks in turbulent wall-bounded shear flow, J. Fluid Mech. **708**, 149 (2012).

[28] J. R. Herring, Investigation of problems in thermal convection, J. Atmos. Sci. **20**, 325 (1963).

[29] N. C. Constantinou, B. F. Farrell, and P. J. Ioannou, Statistical state dynamics of jet-wave coexistence in barotropic beta-plane turbulence, J. Atmos. Sci. **73**, 2229 (2016).

[30] V. Thomas, B. K. Lieu, M. R. Jovanović, B. F. Farrell, P. J. Ioannou, and D. F. Gayme, Self-sustaining turbulence in a restricted nonlinear model of plane Couette flow, Phys. Fluids **26**, 105112 (2014).

[31] M. Nagata, Three-dimensional traveling-wave solutions in plane Couette flow, Phys. Rev. E **55**, 2023 (1997).

[32] P. Hall and F. Smith, On strongly nonlinear vortex/wave interactions in boundary-layer transition, J. Fluid Mech. **227**, 641 (1991).

[33] F. Waleffe, Homotopy of exact coherent structures in plane shear flows, Phys. Fluids **15**, 1517 (2003).

[34] J. Wang, J. Gibson, and F. Waleffe, Lower Branch Coherent States in Shear Flows: Transition and Control, Phys. Rev. Lett. **98**, 204501 (2007).

[35] K. Deguchi, P. Hall, and A. Walton, The emergence of localized vortex-wave interaction states in plane Couette flow, J. Fluid Mech. **721**, 58 (2013).

[36] K. Deguchi and P. Hall, The high-Reynolds-number asymptotic development of nonlinear equilibrium states in plane Couette flow, J. Fluid Mech. **750**, 99 (2014).

[37] K. Deguchi and P. Hall, On the instability of vortex-wave interaction states, J. Fluid Mech. **802**, 634 (2016).

[38] B. F. Farrell and P. J. Ioannou, Structural stability of turbulent jets, J. Atmos. Sci. **60**, 2101 (2003).

[39] B. F. Farrell and P. J. Ioannou, in *Zonal Jets*, edited by B. Galperin and P. L. Read (Cambridge University Press, Cambridge, 2016), Chap. 5.

[40] P. Hall and S. Sherwin, Streamwise vortices in shear flows: Harbingers of transition and the skeleton of coherent structures, J. Fluid Mech. **661**, 178 (2010).

[41] A. Eliassen and E. Palm, On the transfer of energy in stationary mountain waves, Geofys. Publ. **22**(3), 1 (1960).

[42] J. P. Boyd, The noninteraction of waves with the zonally averaged flow on a spherical earth and the interrelationships on eddy fluxes of energy, heat and momentum, J. Atmos. Sci. **33**, 2285 (1976).

[43] D. G. Andrews and M. E. McIntyre, Planetary waves in horizontal and vertical shear: The generalized Eliassen-Palm relation and the mean zonal acceleration, J. Atmos. Sci. **33**, 2031 (1976).

[44] See Supplemental Material at http://link.aps.org/supplemental/10.1103/PhysRevFluids.2.034607 for movies.

[45] N. C. Constantinou, B. F. Farrell, and P. J. Ioannou, Emergence and equilibration of jets in beta-plane turbulence: Applications of stochastic structural stability theory, J. Atmos. Sci. **71**, 1818 (2014).

[46] G. Berkooz, P. Holmes, and J. L. Lumley, The proper orthogonal decomposition in the analysis of turbulent flows, Annu. Rev. Fluid Mech. **25**, 539 (1993).

[47] M.-A. Nikolaidis, B. F. Farrell, P. J. Ioannou, D. F. Gayme, A. Lozano-Durán, and J. Jiménez, A POD-based analysis of turbulence in the reduced nonlinear dynamics system, J. Phys.: Conf. Ser. **708**, 012002 (2016).